

Cavity-like strong coupling in macroscopic waveguide QED using three coupled qubits in the deep non-Markovian regime

Sofia Arranz Regidor^{1,*} and Stephen Hughes¹

¹*Department of Physics, Engineering Physics and Astronomy,
Queen's University, Kingston, Ontario, Canada, K7L 3N6*

(Dated: July 2, 2021)

We introduce a three qubit waveguide QED system to mimic the cavity-QED strong coupling regime of a probe qubit embedded in atom-like mirrors, which was realized in recent experiments. We then extend this system into the deep non-Markovian regime and demonstrate the profound role that retardation plays on the dressed resonances, allowing one to significantly improve the polariton lifetimes (by many orders of magnitude), tune the resonances, as well as realize Fano-like resonances and simultaneous coupling to multiple cavity modes. Exact Green function solutions are presented for the spectral resonances, and the quantum dynamics are simulated using matrix product states, where we demonstrate additional control of the cavity-QED system using chiral probe qubits. We also show example qubit dynamics with both one and two quantum excitations.

Introduction.—Cavity-QED phenomena have been studied both theoretically and experimentally for various cavity systems (e.g., see Refs. [1–17]), showing a variety of applications and rich quantum physics. These cavity systems are typically characterized by Markovian decay dynamics, where interactions between system operators are essentially instantaneous. One of the key signatures of such systems is the “strong coupling” regime, where the intrinsic quantum coherence overcomes system losses.

A fundamentally different dynamic can be realized using waveguide QED systems [18–27], which allow one to efficiently couple quantum emitters and two level systems acting as qubits, over macroscopic length scales. Here the waveguide modes mediate the photon coupling between the qubits, and the system can have a non-Markovian memory [28–32]. Coherent feedback systems can thus lead to non-trivial dynamical protocols such as population trapping, and photon transport beyond the usual dipole-dipole interaction regimes [33–35]. For example, these waveguide-QED regimes can be experimentally realized in chip-based systems with semiconductor quantum dots and semiconducting circuits [25, 36, 37].

It is interesting to explore when these two disparate systems (cavities and waveguides) overlap with each other, in terms of the connecting physics, and in particular if one can realize familiar cavity-QED phenomena with richer non-Markovian dynamics than what is often assumed with traditional cavities. To help address this question, recently it was experimentally demonstrated how one can achieve cavity-QED phenomena, such as vacuum Rabi oscillations and qubit *strong coupling*, by simply having some of the qubits act as “atom-like mirrors” [38, 39]. A schematic representation of this scenario is shown in Fig. 1, where a *probe qubit* is situated between two external *mirror qubits*. Reference [38] showed how the *usual* strong coupling regime can be reached by precisely positioning the external qubits, which can behave

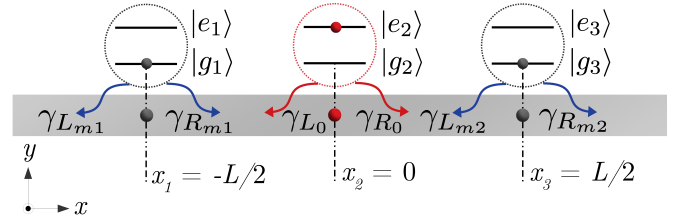


Figure 1. Schematic of three qubits on a waveguide.

as a collective entangled state, creating a cavity-like system. This regime is mediated by coherent qubit interactions [38]. This recent experimental achievement allows one to manipulate correlated dissipation and coherence of quantum emitter arrays, with engineerable feedback. Strong coupling dynamics have also been theoretically demonstrated for qubits at a waveguide mode edge [40].

Motivated by these emerging experiments on tunable quantum networks, here we present a study of qubit-mirrors in the *deep non-Markovian regime*, and show how longer time delays between the qubits result in much richer coupling dynamics than traditional cavity-QED, yielding spectrally narrow linewidths and the simultaneous coupling to multiple cavity modes for sufficiently long round trip times. We first employ a classical scattering theory, solving for the exact Green function to analyze the spectral resonances beyond the Markovian approximation, in a strong coupling regime. We find that the main two Rabi split resonances (from an infinite set) depend on the mirror-qubit delay times, which significantly narrow when the retardation increases, and recover the Markovian limit solution only for small delay times. We show explicitly how a non-Markovian delay time significantly improves the cavity-QED resonances. We also study this problem from the viewpoint of matrix products states (MPS), which allows us to solve the quantum Hamiltonian also in the non-Markovian regime [41] as well as the nonlinear regime. We directly show how the lifetimes *improve dramatically* for long delay times when the retardation is considered, giving a method to pre-

* 18sar4@queensu.ca

cisely control the coherence times of these novel polariton states. In addition, we investigate the time dynamics for a chiral probe qubit [42, 43], and explore qubit dynamics with one and two initial quantum excitations.

Classical Scattering Theory.—Light propagation through an arbitrary dielectric medium can be described in terms of the mode solutions to the Helmholtz equation: $\nabla \times \nabla \times \mathbf{f}_\lambda(\mathbf{r}) - \frac{\omega^2}{c^2} \epsilon(\mathbf{r}) \mathbf{f}_\lambda(\mathbf{r}) = 0$, where $\epsilon(\mathbf{r})$ describes the relative permittivity of the structure and $\mathbf{f}_\lambda(\mathbf{r})$ are generalized field modes with a harmonic $e^{-i\omega t}$ time dependence. For the waveguide, we consider a photonic nanowire, supporting lossless waveguide modes $\mathbf{f}_{k_\omega}(\mathbf{r}) = \sqrt{\frac{1}{L_W}} \mathbf{e}_{k_\omega}(\boldsymbol{\rho}) e^{ik_\omega x}$, with $\mathbf{e}_{k_\omega}(\boldsymbol{\rho})$ the mode solution, normalized from $\int_{A_w} \epsilon(\boldsymbol{\rho}) \mathbf{e}_{k_\omega}^*(\boldsymbol{\rho}) \cdot \mathbf{e}_{k'_\omega}(\boldsymbol{\rho}) = \delta_{k_\omega, k'_\omega}$, where A_w is the spatial area, and L_W is the length of the waveguide. The waveguide Green function is [44]

$$\mathbf{G}_w(\mathbf{r}, \mathbf{r}', \omega) = \frac{i\omega}{2v_g} \left[\Theta(x - x') \mathbf{e}_{k_\omega}(\boldsymbol{\rho}) \mathbf{e}_{k_\omega}^*(\boldsymbol{\rho}') e^{ik_\omega(x-x')} + \Theta(x' - x) \mathbf{e}_{k_\omega}^*(\boldsymbol{\rho}) \mathbf{e}_{k_\omega}(\boldsymbol{\rho}') e^{ik_\omega(x'-x)} \right], \quad (1)$$

where the terms preceded by Heaviside functions correspond to forward and backwards propagating modes, respectively, and v_g is the group velocity at the frequency on interest. Since the modes are translationally invariant in x , then $\mathbf{e}_{k_\omega}(\mathbf{r}) = \mathbf{e}_{k_\omega}(\boldsymbol{\rho})$. The notation can be easily generalized for photonic crystal waveguides [44].

Next, we consider adding in a single qubit treated at the level of a polarization dipole. The polarizability of the qubit, with resonance energy ω_0 , is described through the polarizability tensor $\boldsymbol{\alpha}_0 = \alpha_0 \mathbf{n}_d \mathbf{n}_d^\dagger$, where \mathbf{n}_d is a unit vector describing the polarization direction of the qubit dipole, and $\alpha_0 = A_0 \omega^2 / (\omega_0^2 - \omega^2)$ is the ‘‘bare polarizability’’ volume [45], i.e., it does not include radiative coupling effects to the environment, and $A_0 = 2\omega_p d_0^2 / \epsilon_0 \hbar$.

The total electric field in the waveguide is (ω is implicit) $\mathbf{E}(\mathbf{r}) = \mathbf{E}^h(\mathbf{r}) + \mathbf{G}(\mathbf{r}, \mathbf{r}_d) \cdot \boldsymbol{\alpha}_0 \cdot \mathbf{E}(\mathbf{r}_d)$, where $\boldsymbol{\alpha}_0$ has units of volume, \mathbf{r}_d is the position of the qubit, $\mathbf{E}^h(\mathbf{r})$ is the homogeneous field solution in the absence of the qubits. It is also convenient to exploit the Dyson equation, $\mathbf{G}^{(1)} = \mathbf{G} + \mathbf{G} \cdot \boldsymbol{\alpha}_0 \cdot \mathbf{G}^{(1)}$, where the ‘1’ superscript denotes the GF with the addition of one qubit, so that

$$\mathbf{E}(\mathbf{r}) = \mathbf{E}^h(\mathbf{r}) + \mathbf{G}^{(1)}(\mathbf{r}, \mathbf{r}_d) \cdot \boldsymbol{\alpha}_0 \cdot \mathbf{E}^h(\mathbf{r}_d), \quad (2)$$

where $\mathbf{G}^{(1)}(\mathbf{r}, \mathbf{r}') = \mathbf{G}(\mathbf{r}, \mathbf{r}') / (1 - \alpha_0 \mathbf{n}_d^\dagger \cdot \mathbf{G}_d \cdot \mathbf{n}_d)$. Alternatively, one can introduce the renormalized polarizability, $\boldsymbol{\alpha}^{(1)} = \boldsymbol{\alpha}_0 + \boldsymbol{\alpha}_0 \cdot \mathbf{G}_d \cdot \boldsymbol{\alpha}$, with $\mathbf{G}_d \equiv \mathbf{G}(\mathbf{r}_d, \mathbf{r}_d)$. The polarizability, including coupling to the medium is

$$\boldsymbol{\alpha}^{(1)} = \frac{A_0 \omega_0^2 \mathbf{n}_d \mathbf{n}_d^\dagger}{\omega_0^2 - \omega^2 - i\omega_0 \gamma}, \quad (3)$$

where $\gamma = A_0 \omega_0 \mathbf{n}_d^\dagger \cdot \text{Im} \mathbf{G}_d \cdot \mathbf{n}_d = \gamma_L + \gamma_R$, and we assume the qubit is symmetrically coupled to both forward and backwards modes (unless stated otherwise). It is also useful to define the normalized scattered field at the qubit, from $\tilde{E}_s^{(1)}(\mathbf{r}_d) = \boldsymbol{\alpha}_0 \cdot \mathbf{G}^{(1)}(\mathbf{r}_d, \mathbf{r}_d) \cdot \mathbf{n}_d$.

Next we consider an injected waveguide mode from the left, $\mathbf{E}^h(\mathbf{r}) = \mathbf{f}_{k_h}(\mathbf{r}) = \sqrt{\frac{1}{L_W}} \mathbf{e}_{k_h}(\mathbf{r}) e^{ik_h x}$. The reflection coefficient from one qubit is

$$r_1(\omega) = \frac{\mathbf{E}_r(\mathbf{r}; x \rightarrow -\infty)}{\mathbf{E}^h(\mathbf{r}; x \rightarrow -\infty)} = \frac{i\omega_0 \gamma e^{i\phi(x_d)}}{\omega_0^2 - \omega^2 - i\omega_0 \gamma}, \quad (4)$$

where \mathbf{E}_r is the reflected field, and $\phi(x_d)$ is a positional dependent phase; the transmission coefficient can be derived in a similar way. Thus, we see that the waveguide qubit indeed acts as a mirror, with a Lorentzian line-shape, whose spectral width is determined by the radiation decay rate. The strategy for obtaining atom-like mirrors then becomes clear: we can surround a single qubit with two mirror qubit and expect the system to mimic a Fabry-Pérot resonator. To make this clearer, we now add in another qubit, acting as a second resonant mirror, separated from the first by a distance L . Assuming identical mirror qubits, we can use the Dyson equation again to derive the total reflection coefficient as

$$r_{2\text{dots}}(\omega) = \frac{r_1(\omega) [1 + e^{2ikL} + 2r_1(\omega) e^{2ikL}]}{1 - r_1^2(\omega) e^{2ikL}}, \quad (5)$$

which is precisely the solution expected from a 1d cavity with two identical mirrors with a complex reflection coefficient, r_1 . For simplicity, he have neglected the mirror phase terms. The *mirror* round trip time is $\tau_{RT} = n_g L / c = 2\tau$ (with n_g the group index), which will yield cavity modes with a free spectral range (FSR) $\Delta\omega_{FSR} \approx 2\pi / \tau_{RT}$. Note if we make a rotating wave approximation, $\omega_0^2 - \omega^2 \approx 2\omega_0(\omega_0 - \omega)$, then we recover the quantum mechanically derived results [46].

We next add in a probe (third) qubit, also with $\omega_p = \omega_0$, and use the Dyson equation again to derive an explicit solution for the Green function and for the scattered fields. At the probe qubit (\mathbf{r}_p), we have

$$\tilde{E}_s^{(3)}(\mathbf{r}_p) = \boldsymbol{\alpha}_0 \cdot \mathbf{G}^{(3)}(\mathbf{r}_p, \mathbf{r}_p) \cdot \mathbf{n}_p = \frac{i\omega_p \tilde{\gamma}_p}{\omega_p^2 - \omega^2 - i\omega \tilde{\gamma}_p}, \quad (6)$$

with the modified decay rate

$$\tilde{\gamma}_p = \gamma_p \left[1 + e^{ikL} r_1(\omega) + (e^{ikL/2} + e^{ikL/2} e^{ikL} r_1(\omega)) \times \frac{r_1(\omega) (e^{ikL/2} + r_1(\omega) e^{ikL/2} e^{ikL})}{1 - r_1^2(\omega) e^{2ikL}} \right], \quad (7)$$

which is an exact solution. It is also straightforward to derive the scattered field from the mirror qubits, but this solution alone is enough to probe the system resonances.

Strong Coupling Regime.—To connect to the familiar cavity-QED strong coupling regime, we can study the complex poles in Eq. (6). Strong coupling is optimally achieved when the modified probe decay rate approaches infinity, and when $\omega = \omega_0 = \omega_p$, $r_1 \rightarrow -1$. Thus, one needs to satisfy the following phase matching conditions: $e^{i2\omega\tau} \equiv e^{i2kL} = 1$ and $e^{i\omega\tau} = -1$. Neglecting retardation effects (Markov approximation), this is possible

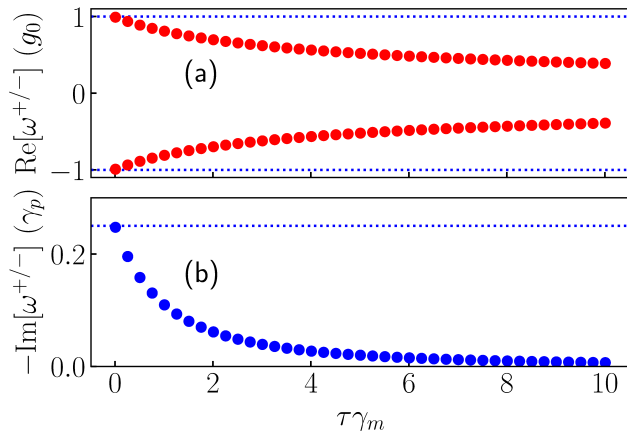


Figure 2. Complex poles of the two main polariton states using Eq. (6) with no approximations. Note that $\tau = \tau_{\text{RT}}/2$, and $\gamma_m = 10\gamma_p$. The dashed lines show the non-retarded solution (Markov) as also identified in the text.

when $\omega_0\tau/2 = m\pi + \pi/2$, which was achieved in Ref. [38] by having $L = \lambda/2$ ($m = 0$), and the probe qubit at cavity center. Using this phase conditions, and a rotating wave approximation, the two main complex roots are:

$$\tilde{\omega}^{\pm} \approx \omega_p - i\frac{\gamma_p}{4} \pm \frac{1}{2}\sqrt{2\gamma_p\gamma_m}, \quad (8)$$

where we assume $\gamma_m \gg \gamma_p$, with γ_m the mirror qubit decay rate. For on-resonance, $\omega = \omega_0$, then $r_1 \rightarrow -1$, and the term in brackets in Eq. (7) tends to infinity, as does the Purcell effect of an immutable dipole. However, in a strong coupling regime, with small τ , the original linewidth is reduced by 50% and there will be a splitting of $\pm g_0$, with $g_0 = \sqrt{2\gamma_m\gamma_p}/2$ [38]. For longer delay times, the polariton states decrease in energy and their lifetime increases, an effect that requires retardation in the model.

Figure 2 shows the first near-resonant complex poles as a function of τ for a decay rate $\gamma_m = 10\gamma_p$. In the Markovian limit, the value of the poles are constant (horizontal dashed lines). However, if the delay times are taken into account (non-Markovian case, symbols), it can be seen how the values of the complex poles decrease as the separation between the atoms increases; thus, the resonances are in fact dependent on the retardation (and other modes can also become important, not shown here); however, in units of g_0 , and using a Markov approximation, the coupling rate is always 1 (splitting of $\pm g_0$), but this only applies for sufficiently short delay times. When the retardation is sufficiently large, we can have $g_{\text{eff}} < 1$ as τ increases, with already notable differences as small as $\tau\gamma_m = 0.1$. In addition, we observe that in the units presented in Fig. 2 ($\tau\gamma_m$), the results look identical for different decay rate ratios (e.g., if $\gamma_m = 100\gamma_p$).

In Fig. 3, we show the reflectivity (blue curve) of the bare two-qubit mirror system as well as the probe qubit scattered field (red curve) for different delay times. For the scattered field, we observe how Rabi splitting decreases and sharpens for longer delay times. In contrast,

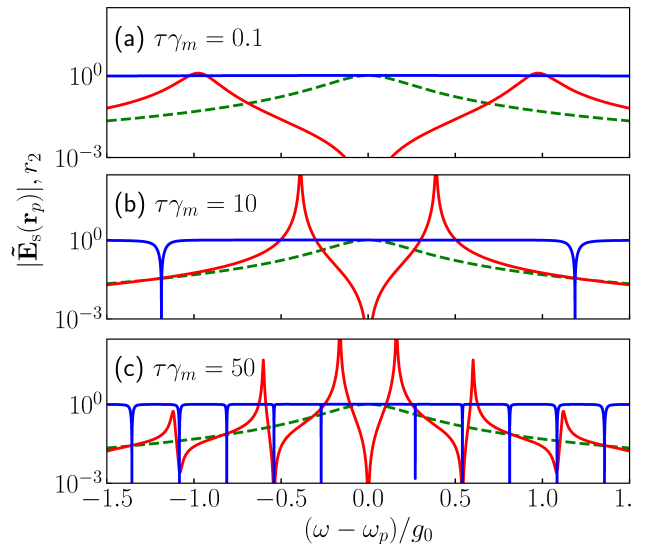


Figure 3. Scattered field (red curve) and two qubit reflectivity (blue curve) at the probe dot for various delay times, using $\gamma_m = 10\gamma_p$. (a) $\tau\gamma_m = 0.1$; (b) $\tau\gamma_m = 10$; (c) $\tau\gamma_m = 50$. The green dashed curve shows the single qubit scattered field.

the single qubit system just displays a Lorentzian line-shape (green curve). In addition, for the longer delay time, we can observe a coupling to the $m = \pm 2, 4$ modes causing a striking Fano resonance [46, 47]; note that the $m = \pm 1, 3$ modes do not couple since the probe qubit is at a node of these cavity modes. For the shorter delay time in (a), the peaks are placed approximately at $\pm g_0$ (slightly decreased), which corresponds close to the Markovian limit result. However, for the longer delay times, in (b) and (c), then clearly the effective Rabi splitting, g_{eff} , becomes smaller for longer delay times. The first cavity sideband resonance in (b) and (c) are at $\omega_{c1} = 1.19g_0$ and $0.27g_0$, respectively; and note that these are also influenced by the dispersion in $r_1(\omega)$. Also note that $\omega_{c1}/g_0 \propto \sqrt{\gamma_m/\gamma_p}$.

Quantum Theory using Matrix Products States (MPSs).—To represent the time evolution of the probe qubit in the non-Markovian regime, and to confirm our semiclassical results in the frequency domain, we next solve the same system using MPSs [48–50]. To do this, we first consider the Hamiltonian for three qubits [41],

$$H = \sum_{n=1,2,3} \omega_n \sigma_n^+ \sigma_n^- + \sum_{\alpha=L,R} \int_{-\infty}^{\infty} d\omega \omega b_{\alpha}^{\dagger}(\omega) b_{\alpha}(\omega) + H_{\text{I}}, \quad (9)$$

where ω_n are the resonant frequencies and σ_n^{\pm} are the Pauli operators of the qubits, and $b_{\alpha}(\omega)$ is the frequency dependent boson operator. The interaction term,

$$H_{\text{I}} = \frac{1}{\sqrt{2\pi}} \int_{-\infty}^{\infty} d\omega \left\{ \sum_{n=1,2,3} (\sqrt{\gamma_n^L} e^{i\omega x_n/c} b_L(\omega) \sigma_n^+ + \sqrt{\gamma_n^R} e^{-i\omega x_n/c} b_R(\omega) \sigma_n^+) + \text{H.c.} \right\}, \quad (10)$$

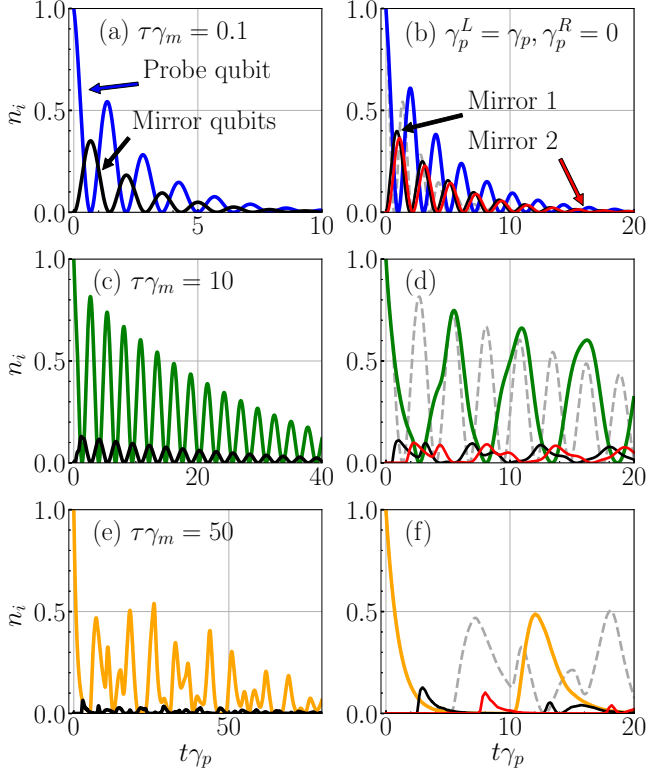


Figure 4. Probe and mirror population dynamics using $n_p(0) = 1$ in vacuum, where again we use $\gamma_m = 10\gamma_p$, for the same three delay times shown in Fig. 3: (blue) $\tau\gamma_m = 0.1$; (green) $\tau\gamma_m = 10$; (orange) $\tau\gamma_m = 50$. Cases (a,c,e) are the symmetric examples corresponding to the ones studied in Fig. 3 in the frequency domain, where $\gamma_p^L = \gamma_p^R = \gamma_p/2$. Subplots (b,d,f) show the same time dynamics when the probe qubit is chiral, with $\gamma_p^L = \gamma_p$ and $\gamma_p^R = 0$. The grey dashed line is the corresponding symmetric case for comparison.

where x_n are the positions of the atoms, and γ_n^L, γ_n^R represent the left and right decay rates, respectively. Choosing a rotating frame corresponding to the center (probe) qubit frequency, and defining the boson operators in the time domain, the Hamiltonian can be written as

$$\begin{aligned}
 H = & \Delta_m \sigma_1^+ \sigma_1^- + \Delta_m \sigma_3^+ \sigma_3^- \\
 & + \sqrt{\gamma_m} (e^{i\omega_0 \tau} b_L(t-\tau) + b_R(t)) \sigma_1^+ + \text{H.c.} \\
 & + \sqrt{\gamma_p} (e^{i\omega_0 \tau/2} b_L(t-\tau/2) + e^{i\omega_0 \tau/2} b_R(t-\tau/2)) \sigma_2^+ + \text{H.c.} \\
 & + \sqrt{\gamma_m} (b_L(t) + e^{i\omega_0 \tau} b_R(t-\tau)) \sigma_3^+ + \text{H.c.}, \quad (11)
 \end{aligned}$$

where we have considered symmetric decay rates, with $\gamma_1 = \gamma_3 = \gamma_m$, $\gamma_2 = \gamma_p$, and the probe qubit is situated in the middle; $\Delta_m = \omega_m - \omega_0$ where ω_m is the frequency of the external qubits. For the cases considered, all qubits are on resonance and $\Delta_m = 0$. Equation (11) allows us to write the time evolution operator in the MPS repre-

sentation as a matrix product operator [51],

$$\begin{aligned}
 U(t_k, t_{k+1}) = & \exp[-i\sqrt{\gamma_m} (e^{i\omega_0 \tau} \tilde{B}_L(t_{k-1}) + \tilde{B}_R(t_k)) \sigma_1^+ \\
 & + \text{H.c.} - i\sqrt{\gamma_p} (e^{i\omega_0 \tau/2} \tilde{B}_L(t_{k-1/2}) \\
 & + e^{i\omega_0 \tau/2} \tilde{B}_R(t_{k-1/2})) \sigma_2^+ + \text{H.c.} \\
 & - i\sqrt{\gamma_m} (\tilde{B}_L(t_k) + e^{i\omega_0 \tau} \tilde{B}_R(t_{k-1}))], \quad (12)
 \end{aligned}$$

where \tilde{B} is the time-bin bosonic noise operator [33, 34].

Following this procedure, the cases shown in Fig. 3 are studied in the time domain and the evolution of the probe dot population ($n_p(t) = \langle \sigma_2^+ \sigma_2^- \rangle(t)$) is represented in Figs. 4 (a,c,e), and similarly for the mirror qubit populations. Vacuum Rabi oscillations are present in all the cases. It is also observed that *significantly larger decay rates appear for the probe dot for the longer delay time* in (c) compared to (a), while the dynamics in (e) ($\tau\gamma_m = 50$) results in a high degree of interference because the qubit resonance now couples to the multiple cavity modes. In addition, population evolution of the mirror qubits is shown in black (both mirror qubits show the same population). We observe that this population stays closer to zero for longer delay times, and in (e) the interference is also reflected in the mirror dots.

We next show further control of this waveguide cavity-QED system by considering a chiral probe qubit with $\gamma_p^L = \gamma_p$ and $\gamma_p^R = 0$. Chiral systems allow direction-dependent coupling, offering multiple applications in quantum networks (e.g., see Refs. [42, 52, 53]). In Figs. 4 (b,d,f), we show the time evolution for similar systems as before but now considering the chiral probe qubit. In this case, the photons only interact with the probe dot when they are reflected from the right mirror. We also observe a variation of the time evolution with a further improvement of the coherence times. In addition, the mirror qubits results do not match as we have broken the symmetry of the system, and it can be seen that, when the delay times increase, the separation between the same peak for each mirror increases, showing very clearly the influence of the retardation on the chiral qubit dynamics.

Finally, we consider a double excitation (nonlinear) case by also starting an excitation in one of the mirrors (mirror 1 in Fig. 5). Here, we compare this new case with the one shown previously with just one excitation. For this example, we choose the decay rate of $\gamma_m = 10\gamma_p$ and a feedback $\tau\gamma_m = 1$. In Fig. 5(a,b), we show the symmetric coupling case ($\gamma_p^L = \gamma_p^R = \gamma_p/2$) and observe how the values of n_p change but the oscillation period is similar. A significantly faster initial decay of the mirror qubit is seen in (b) due to the larger decay rate of the mirror qubits. Then we study the chiral cases, with $\gamma_p^L = \gamma_p$ and $\gamma_p^R = 0$ in (c,d), and $\gamma_p^L = 0$ and $\gamma_p^R = \gamma_p$ in (e,f). In (c,e), the mirror qubit are exchanged and the probe qubit behaves similarly. However, in the double excited cases (d,f), we can see that not only does n_p vary but also the position of the peaks changes. In (d), only the photons coming from the right mirror (mirror 2) interact with the probe qubit, while in (f) the photons interacting

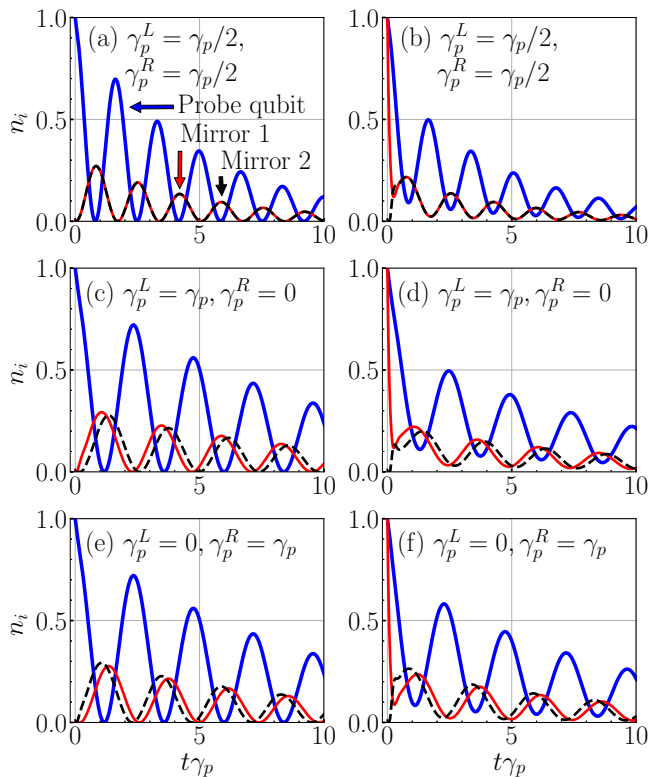


Figure 5. Probe and mirror population dynamics using one excitation ($n_p(0) = 1$) in vacuum for (a,c,e), and two excitations ($n_p(0) = 1$, $n_{m1}(0) = 1$) in vacuum for (b,d,f). In all cases $\gamma_m = 10\gamma_p$, for a delay time $\tau\gamma_m = 1$. Subplots (c,d,e,f) show the time dynamics when the probe qubit is chiral, with $\gamma_p^L = \gamma_p$ and $\gamma_p^R = 0$ in (c,d), and $\gamma_p^L = 0$ and $\gamma_p^R = \gamma_p$ in (e,f). Although probe qubit behaves similarly in (c,e), the double excitation breaks the symmetry giving rise to different quantum dynamics in (d,f).

with the probe qubit are the ones coming from the left one (mirror 1). This leads to higher values of n_p in (f), and a phase difference between both scenarios.

Conclusions.—We have introduced a theory of qubit-like mirrors which mimics cavity-QED interactions, consistent with recent experiments. We then extended this system into a much richer dynamical coupling regime, by introducing retardation through a finite round trip memory, which increases the lifetime of the cavity-qubit polariton states by several orders of magnitude, while also reducing the overall vacuum Rabi splitting. For sufficiently long delays, we demonstrated how several cavity modes can act in concert, producing non-trivial and highly non-Markovian population dynamics of a probe qubit. Our theory first presented an analytical solution to the semiclassical problem of three dipoles in a waveguide, using an exact Green function. This picture was complemented by using MPS, where we showed the population dynamics including an example for an embedded chiral probe qubit. In both theoretical pictures, we explicitly showed how to increase the lifetime of the polariton states by increasing the delay time between the external qubit mirrors. In addition, we demonstrated the role of several quantum excitations in a nonlinear regime, showing significantly faster early time decay. These retardation effects also facilitate the exploration of quantum nonlinear cavity-QED effects with coherent driving fields using engineerable multiple qubits in waveguides.

Acknowledgements.—We acknowledge funding from the Canadian Foundation for Innovation (CFI), Queen’s University and the Natural Sciences and Engineering Research Council of Canada (NSERC).

-
- [1] S. Ashhab and F. Nori, Qubit-oscillator systems in the ultrastrong-coupling regime and their potential for preparing nonclassical states, *Phys. Rev. A* **81**, 042311 (2010).
- [2] D. D. Sedov, V. K. Kozin, and I. V. Iorsh, Chiral waveguide optomechanics: First order quantum phase transitions with z_3 symmetry breaking, *Phys. Rev. Lett.* **125**, 263606 (2020).
- [3] A. Kuhn, M. Hennrich, and G. Rempe, Deterministic single-photon source for distributed quantum networking, *Phys. Rev. Lett.* **89**, 067901 (2002).
- [4] Y. Zhu, D. J. Gauthier, S. E. Morin, Q. Wu, H. J. Carmichael, and T. W. Mossberg, Vacuum Rabi splitting as a feature of linear-dispersion theory: Analysis and experimental observations, *Phys. Rev. Lett.* **64**, 2499 (1990).
- [5] S. Sharnailov, A. Parkins, M. Collett, and H. Carmichael, Multi-photon blockade and dressing of the dressed states, *Optics Communications* **283**, 766 (2010).
- [6] C. Leroux, L. C. G. Govia, and A. A. Clerk, Enhancing cavity quantum electrodynamics via antisqueezing: Synthetic ultrastrong coupling, *Phys. Rev. Lett.* **120**, 093602 (2018).
- [7] W. Qin, A. Miranowicz, P.-B. Li, X.-Y. Lü, J. Q. You, and F. Nori, Exponentially enhanced light-matter interaction, cooperativities, and steady-state entanglement using parametric amplification, *Phys. Rev. Lett.* **120**, 093601 (2018).
- [8] L. Garziano, R. Stassi, V. Macrì, A. F. Kockum, S. Savasta, and F. Nori, Multiphoton quantum Rabi oscillations in ultrastrong cavity QED, *Phys. Rev. A* **92**, 063830 (2015).
- [9] T. Yoshie, A. Scherer, J. Hendrickson, G. Khitrova, H. M. Gibbs, G. Rupper, C. Ell, O. B. Shchekin, and D. G. Deppe, Vacuum Rabi splitting with a single quantum dot in a photonic crystal nanocavity, *Nature* **432**, 200 (2004).
- [10] J. P. Reithmaier, G. Sęk, A. Löffler, C. Hofmann, S. Kuhn, S. Reitzenstein, L. V. Keldysh, V. D. Kulakovskii, T. L. Reinecke, and A. Forchel, Strong coupling in a single quantum dot–semiconductor microcavity system, *Nature* **432**, 197 (2004).

- [11] E. Peter, P. Senellart, D. Martrou, A. Lemaître, J. Hours, J. M. Gérard, and J. Bloch, Exciton-photon strong-coupling regime for a single quantum dot embedded in a microcavity, *Phys. Rev. Lett.* **95**, 067401 (2005).
- [12] M. Brune, F. Schmidt-Kaler, A. Maali, J. Dreyer, E. Hagley, J. M. Raimond, and S. Haroche, Quantum Rabi oscillation: A direct test of field quantization in a cavity, *Phys. Rev. Lett.* **76**, 1800 (1996).
- [13] I. Schuster, A. Kubanek, A. Fuhrmanek, T. Puppe, P. W. H. Pinkse, K. Murr, and G. Rempe, Nonlinear spectroscopy of photons bound to one atom, *Nature Physics* **4**, 382 (2008).
- [14] L. S. Bishop, J. M. Chow, J. Koch, A. A. Houck, M. H. Devoret, E. Thuneberg, S. M. Girvin, and R. J. Schoelkopf, Nonlinear response of the vacuum Rabi resonance, *Nature Physics* **5**, 105 (2008).
- [15] J. M. Fink, M. Göppl, M. Baur, R. Bianchetti, P. J. Leek, A. Blais, and A. Wallraff, Climbing the Jaynes–Cummings ladder and observing its nonlinearity in a cavity QED system, *Nature* **454**, 315 (2008).
- [16] D. Englund, A. Majumdar, A. Faraon, M. Toishi, N. Stoltz, P. Petroff, and J. Vučković, Resonant excitation of a quantum dot strongly coupled to a photonic crystal nanocavity, *Phys. Rev. Lett.* **104**, 073904 (2010).
- [17] D. Press, S. Götzinger, S. Reitzenstein, C. Hofmann, A. Löffler, M. Kamp, A. Forchel, and Y. Yamamoto, Photon antibunching from a single quantum-dot-microcavity system in the strong coupling regime, *Phys. Rev. Lett.* **98**, 117402 (2007).
- [18] S. Hughes, Enhanced single-photon emission from quantum dots in photonic crystal waveguides and nanocavities, *Opt. Lett.* **29**, 2659 (2004).
- [19] J. T. Shen and S. Fan, Coherent photon transport from spontaneous emission in one-dimensional waveguides, *Opt. Lett.* **30**, 2001 (2005).
- [20] H. Zheng, D. J. Gauthier, and H. U. Baranger, Waveguide QED: Many-body bound-state effects in coherent and fock-state scattering from a two-level system, *Phys. Rev. A* **82**, 063816 (2010).
- [21] P. Longo, P. Schmitteckert, and K. Busch, Few-photon transport in low-dimensional systems, *Phys. Rev. A* **83**, 063828 (2011).
- [22] J. Román-Roche, E. Sánchez-Burillo, and D. Zueco, Bound states in ultrastrong waveguide QED, *Phys. Rev. A* **102**, 023702 (2020).
- [23] D. Roy, Few-photon optical diode, *Phys. Rev. B* **81**, 155117 (2010).
- [24] D. Roy, C. M. Wilson, and O. Firstenberg, Colloquium: Strongly interacting photons in one-dimensional continuum, *Rev. Mod. Phys.* **89**, 021001 (2017).
- [25] A. Rosario Hamann, C. Müller, M. Jerger, M. Zanner, J. Combes, M. Pletyukhov, M. Weides, T. M. Stace, and A. Fedorov, Nonreciprocity realized with quantum nonlinearity, *Phys. Rev. Lett.* **121**, 123601 (2018).
- [26] S. J. Masson and A. Asenjo-Garcia, Atomic-waveguide quantum electrodynamics, *Phys. Rev. Research* **2**, 043213 (2020).
- [27] A. S. Sheremet, M. I. Petrov, I. V. Iorsh, A. V. Poshakinskiy, and A. N. Poddubny, Waveguide quantum electrodynamics: collective radiance and photon-photon correlations (2021), [arXiv:2103.06824](https://arxiv.org/abs/2103.06824).
- [28] K. Sinha, P. Meystre, E. A. Goldschmidt, F. K. Fatemi, S. L. Rolston, and P. Solano, Non-Markovian collective emission from macroscopically separated emitters, *Phys. Rev. Lett.* **124**, 043603 (2020).
- [29] S. Longhi, Rabi oscillations of bound states in the continuum, *Opt. Lett.* **46**, 2091 (2021).
- [30] L. Du, M.-R. Cai, J.-H. Wu, Z. Wang, and Y. Li, Single-photon nonreciprocal excitation transfer with non-Markovian retarded effects, *Phys. Rev. A* **103**, 053701 (2021).
- [31] L. Guo, A. F. Kockum, F. Marquardt, and G. Johansson, Oscillating bound states for a giant atom, *Phys. Rev. Research* **2**, 043014 (2020).
- [32] S. Longhi, Superradiance paradox in waveguide lattices, *Opt. Lett.* **45**, 3297 (2020).
- [33] H. Pichler and P. Zoller, Photonic circuits with time delays and quantum feedback, *Phys. Rev. Lett.* **116**, 093601 (2016).
- [34] S. Arranz Regidor, G. Crowder, H. Carmichael, and S. Hughes, Modeling quantum light-matter interactions in waveguide QED with retardation, nonlinear interactions, and a time-delayed feedback: Matrix product states versus a space-discretized waveguide model, *Phys. Rev. Research* **3**, 023030 (2021).
- [35] G. Crowder, H. Carmichael, and S. Hughes, Quantum trajectory theory of few-photon cavity-QED systems with a time-delayed coherent feedback, *Physical Review A* **101**, 023807 (2020).
- [36] X. Gu, A. F. Kockum, A. Miranowicz, Y. xi Liu, and F. Nori, Microwave photonics with superconducting quantum circuits, *Physics Reports* **718–719**, 1 (2017).
- [37] A. F. Kockum, G. Johansson, and F. Nori, Decoherence-free interaction between giant atoms in waveguide quantum electrodynamics, *Phys. Rev. Lett.* **120**, 140404 (2018).
- [38] M. Mirhosseini, E. Kim, X. Zhang, A. Sipahigil, P. B. Dieterle, A. J. Keller, A. Asenjo-Garcia, D. E. Chang, and O. Painter, Cavity quantum electrodynamics with atom-like mirrors, *Nature* **569**, 692 (2019).
- [39] D. E. Chang, L. Jiang, A. V. Gorshkov, and H. J. Kimble, Cavity QED with atomic mirrors, *New Journal of Physics* **14**, 063003 (2012).
- [40] T. Chen and R.-B. Liu, Non-Markovian dynamics and strong coupling between atomic transitions and a waveguide continuum edge, *Phys. Rev. A* **85**, 043830 (2012).
- [41] A. Carmele, N. Nemet, V. Canela, and S. Parkins, Pronounced non-Markovian features in multiply excited, multiple emitter waveguide QED: Retardation induced anomalous population trapping, *Phys. Rev. Research* **2**, 013238 (2020).
- [42] A. B. Young, A. C. T. Thijssen, D. M. Beggs, P. Androviatsaneas, L. Kuipers, J. G. Rarity, S. Hughes, and R. Oulton, Polarization engineering in photonic crystal waveguides for spin-photon entanglers, *Phys. Rev. Lett.* **115**, 153901 (2015).
- [43] P. Lodahl, S. Mahmoodian, S. Stobbe, A. Rauschenbeutel, P. Schneeweiss, J. Volz, H. Pichler, and P. Zoller, Chiral quantum optics, *Nature* **541**, 473 (2017).
- [44] V. S. C. Manga Rao and S. Hughes, Single quantum-dot Purcell factor and β factor in a photonic crystal waveguide, *Phys. Rev. B* **75**, 205437 (2007).
- [45] P. de Vries, D. V. van Coevorden, and A. Lagendijk, Point scatterers for classical waves, *Rev. Mod. Phys.* **70**, 447 (1998).
- [46] M.-T. Cheng, J. Xu, and G. S. Agarwal, Waveguide transport mediated by strong coupling with atoms, *Phys. Rev. A* **95**, 053807 (2017).

- [47] M. F. Limonov, M. V. Rybin, A. N. Poddubny, and Y. S. Kivshar, Fano resonances in photonics, *Nature Photonics* **11**, 543 (2017).
- [48] C. Yang, F. C. Binder, V. Narasimhachar, and M. Gu, Matrix product states for quantum stochastic modeling, *Physical Review Letters* **121**, 260602 (2018).
- [49] L. Vanderstraeten, *Tensor Network States and Effective Particles for Low-Dimensional Quantum Spin Systems* (Springer, Cham, 2017).
- [50] R. Orús, A practical introduction to tensor networks: Matrix product states and projected entangled pair states, *Annals of Physics* **349**, 117 (2014).
- [51] C. Hubig, I. P. McCulloch, and U. Schollwöck, Generic construction of efficient matrix product operators, *Phys. Rev. B* **95**, 035129 (2017).
- [52] S. Mahmoodian, P. Lodahl, and A. S. Sørensen, Quantum networks with chiral-light-matter interaction in waveguides, *Phys. Rev. Lett.* **117**, 240501 (2016).
- [53] M. J. Mehrabad, A. P. Foster, R. Dost, E. Clarke, P. K. Patil, A. M. Fox, M. S. Skolnick, and L. R. Wilson, Chiral topological photonics with an embedded quantum emitter, *Optica* **7**, 1690 (2020).